Partial Differential Equations in Applied Mathematics 12 (2024) 100988

Contents lists available at ScienceDirect

Partial Differential Equations in Applied Mathematics

journal homepage: www.elsevier.com/locate/padiff

Comparative analysis on the radiative time-dependent water/kerosene-based Cu nanofluid through squeezing Riga plates with heat dissipation: Spectral quasilinearization technique

Subhajit Panda [a], Titilayo M Agbaje [b], Rupa Baithalu [c], S.R. Mishra [c,*]

[a] Centre for Data Science, Siksha 'O' Anusandhan Deemed to be University, Bhubaneswar, Odisha 751030, India
[b] School of Computer Science and Applied Mathematics, University of the Witwatersrand, Johannesburg, Private Bag 3, Braamfontein, 2050, South Africa
[c] Department of Mathematics, Siksha 'O' Anusandhan Deemed to be University, Bhubaneswar, Odisha 751030, India

ARTICLE INFO

Keywords:
Water/kerosene-based Cu nanofluid
Parallel squeezing Riga plates
Darcy dissipation
Thermal convective conditions
Spectral quasilinearization method

ABSTRACT

The time-dependent thermal management along with convective flows are vital in various heat transfer applications in engineering systems such as in automotive cooling systems, and industrial heat exchangers. Because of enhanced thermal conductivity, nanofluids are widely considered for advanced cooling systems such as electronics, aerospace, geothermal energy extraction, etc. The current analysis presents comparative results of the radiative, time-dependent flow of water/kerosene-based Copper nanofluids between squeezing Riga plates focusing on heat dissipation. Both the plates are embedded within a porous matrix and the influence of non-uniform heat source/sink and thermal convective boundary conditions is examined. Riga plates, generally utilized for their ability to generate electromagnetic fields provide greater control over the fluid flow. The problem designed with the inclusion of aforesaid factors is transformed into a non-dimensional form for the utilization of appropriate similarity functions. Further, the impacts of several effective terms on the flow profiles are presented followed by the numerical solution of the profile obtained using the spectral quasilinearization method. Moreover, some of the outstanding findings are; an increase in the fluid velocity is marked for the separation of the plates but the rate of enhancement in the case of kerosene is more pronounced than that of water. Further, irrespective to the type of fluids, the heat transfer rate enhances for the increasing heat fluid which provides the variation of thermal radiation.

1. Introduction

Nanofluids are engineered colloidal suspensions consisting of nanomolecules dispersed in base fluids such as water, ethylene glycol, or oils. These nanoparticles, typically metals, metal oxides, or carbon-based materials like carbon nanotubes, possess enhanced thermal properties, allowing nanofluids to exhibit significantly improved energy transportation characteristics compared to conventional fluids. Due to their superior thermal conductivity, viscosity, and stability, nanofluids are widely used in applications like cooling systems, heat exchangers, electronic cooling, and biomedical processes. By manipulating particle concentration, shape, and material type, the thermophysical features of nanofluids can be optimized, making them a promising solution in the energy, industrial, and biomedical sectors. Choi[1] anticipated the use of nanoparticles to improve thermal conductivity in various materials. Nanofluids are mixtures of basic fluids and nanoparticles that can adopt numerous shapes, including spherical, rod-like, tubular, and rectangular structures. Nanofluids, which are recognized as an alternative to standard fluids for enhancing heat transmission, are created by dispersing nanoparticles ranging in size from 1 to 100 nanometres in a base fluid. Engine oil, ethylene glycol, blood, polymers, and kerosene are examples of common base fluids since they are widely used in a variety of industries. Metallic nanoparticles such as copper (Cu), silver (Ag), and silicon (Si), as well as oxide nanoparticles like copper oxide (CuO) and aluminum oxide (Al_2O_3), have recently received substantial interest. Mahboobtosi's[2] examined the utilization of a tri-hybrid nanofluid instead of a single nanofluid, with H_2O as the host liquid. Additionally, the governing PDEs were transformed into ODEs, which were solved

* Corresponding author.
E-mail addresses: spanda.math@gmail.com (S. Panda), titilayoagbaje@gmail.com (T.M. Agbaje), rupadhananjaygarnaik@gmail.com (R. Baithalu), satyaranjan_mshr@yahoo.co.in (S.R. Mishra).

https://doi.org/10.1016/j.padiff.2024.100988
Received 1 October 2024; Received in revised form 24 October 2024; Accepted 9 November 2024
Available online 12 November 2024

through the "*fifth-order Runge-Kutta (RK5)*" method. In a Numerous study by Yasir et al.[3] examined the combined involvement of Ohmic heating and nonlinear radiating energy on hybridized material mobility via a permeable, shrinking, and stretching cylinder. Their findings demonstrated that the introduction of hybrid nanoparticles enhanced the energy transportation rate. Finally, it is concluded that growing the nanoparticle volume percentage in hybrid ($Al_2O_3 + Cu/H_2O$) nanofluids enhanced the local Nusselt number and skin friction coefficient. Khan et al.[4] presents a numerical investigation on magneto-polarised flow, focusing on the behavior of Williamson and Maxwell micropolar nanomaterials as they flow via a non-isothermal wedge. Furthermore, the standard PDEs are transmuted into a system of ODEs implanting similarity analysis and solved through MAPLE 23. Krishna and Chamkha[5] investigated the free convection flow of a magneto-nanofluid over a semi-infinite permeable plate, incorporating the effects of rotation, continuous heat source, diffusion-thermo, Hall current, and ion slip.

Parallel squeezing Riga plates involves two parallel plates embedded with electrodes and magnets that produce a Lorentz force. The movement of these plates, either towards or away from each other, creates a squeezing effect that induces a magnetic field. This magnetic field interacts with electrically conductive fluids, such as nanofluids, influencing the flow through electromagnetic forces. The Riga plate setup improves control over both flow and heat transmission by utilizing the Lorentz force, which minimizes turbulence and enhances thermal efficiency. A numerical investigation on a conducting convective heat transfer over a Riga plate is conducted by Hayat et al.[6] However, the heat transport properties are affected by the inclusion of radiating heat due to the inclusion of radiative heat and the first-order chemical effect is exhibited in the solutal transfer equations. The governing equations modelled by the characterizing factors are handled numerically using the "*homotopy analysis method*" and the physical properties are elaborated briefly. Ahmed et al.[7] reported the flow behaviour of H_2O-based carbon nanotube nanofluids over Riga plates, considering the influences of radiant heat and viscous dissipation. The governing nonlinear flow model was developed by introducing suitable dimensionless variables into a system of nonlinear ODEs. To solve the model, both numerical and analytical methods were employed. The numerical solution involved applying the "Runge-Kutta method" after converting the nonlinear system into a first-order initial value problem, while the analytical solution was obtained using the Adomian decomposition method. In the study of Kumar et al.[8] examined the behaviour of a third-grade radiative fluid flow through a permeable medium with a sensor device. Additionally, the "*CattaneoChristov double diffusion model*" was utilized for the modelled of the governing equation of the third-grade fluid flow. Furthermore, entropy generation was investigated in accordance with the second law of thermodynamics, and Darcy's model was used to characterize the behavior of the porous medium. Khan et al.[9] examined bio-convective flow of a viscous nanomaterial via various geometries. Sarfraz and Khan[10] explored the rheological features of gyrotactic microorganisms for a Jeffrey fluid with through a biaxial elastic surface. Hayat et al.[11] examined the Prandtl-Eyring nanomaterial flow in the presence of microbes, analyzing the influence of melting heat, radiation, and dissipation on an elongating sheet.

Darcy dissipation refers to the energy loss in fluid flow through porous medium induced by viscous forces, as described in Darcy's law. This phenomenon is important in many applications that use porous materials, such as groundwater aquifers, oil reservoirs, and filtration systems. As the fluid passes through the porous media, the frictional resistance between the fluid and the porous matrix converts mechanical energy into thermal energy, causing the fluid's temperature to rise and its kinetic energy to decrease. Salahuddin et al.[12] reported Darcy-Forchheimer flow and temperature-dependent viscosity in tangent hyperbolic fluids. Awasis et al.[13] investigated the flow phenomena of Eyring-Powell fluid in the presence of a microcantilever sensor, which provided vital perceptions for developing the field of non-Newtonian fluids. To investigate flow dynamics, the analysis uses a Darcy-Forchheimer porous media. Rasool and Zhang[14] investigated the dynamics of nanofluid flow over a widening surface under Darcy-Forchheimer conditions. Their study revealed that as the porosity factor increases, the fluid experiences greater resistance, resulting in a temperature rise. Dero et al.[15] focused on the flow behavior of a Darcy-Forchheimer hybridized fluid via porous media on a shrinking surface under rotational conditions. Eswaramoorthi et al.[16] explored the flow of Casson and Williamson fluids past over an elongating surface, also under the influence of Darcy-Forchheimer drag forces.

The Spectral Quasilinearization Method (SQLM) is a vigorous numerical approach designed to throw nonlinear differential equations by transforming them into a series of linearized problems. Through iterative resolution of the resulting linear problems, SQLM provides approximate solutions that converge quickly and accurately to the true solution. Its effectiveness in managing complex boundary conditions and nonlinearities makes SQLM an invaluable tool across various domains, including fluid dynamics and heat transfer, for researchers aiming for precise numerical solutions to intricate challenges. Mishra et al.[17] explored the influence of dissipative heat, radiation, and chemical reactions on bio-convection. Their work focuses on the impact of cross-diffusive effects, driven by Brownian motion and thermophoresis, impact flow dynamics. Using similarity transformations, they derived a set of coupled nonlinear non-dimensional equations, which were subsequently solved using the quasilinearization method. Their study illustrates the characteristics of various parameters through graphical representations, analyzing the effects of these factors within defined ranges. Agbaje et al.[18] scrutinized the irreversibility processes in the squeezing flow of a polar hybridised material, where blood serves as the host liquid and copper (Cu) and silver (Ag) nanomolecules. Panda et al.[19] explored the on examining the flow characteristics of water-based CNT cross-hybrid nanofluid over a convectively heated surface. Their investigation explanations for the effects of dissipative heat, thermal radiation, and external heat sources/sinks on heat transfer. The problem is transformed into a non-dimensional form using similarity rules, and the "Spectral Quasilinearization Method (SQLM) "is employed to solve the resulting equations accurately. Mishra et al.[20] discussed the H_2O-based hybridised material containing Al_2O_3 and Cu nanoparticles as it flows via a rotating vertical cone filled with porous medium. The presence of magnetism and radiating heat further complicates the convective flow dynamics. Motsa et al.[22] developed a new spectral local linearization method to address nonlinear boundary layer flow problems, drawing on the foundational quasilinearization concepts established by Bellman and Kalaba.[21] Hayat et al.[23] investigated the complexities of squeezing flow over a Riga plate, incorporating chemical reactions and convective effects, while Zeeshan et al.[24] studied radiative bioconvection in nanofluids between rotating circular plates using a semi-numerical DTM-Padé approach. Expanding on these themes, Yusuf et al.[25] conducted an analysis of nonlinear mixed convective flow under Thomson and Troian slip conditions for $Ag–Cu–TiO_2/H_2O$ hybrid nanofluids over a Riga plate. Yusuf et al.[26] explored double diffusive nonlinear convective MHD unsteady slip-flow regimes in a rectangular channel.

Unrevealing study till dated:

- Limited studies on the kerosene-based nanofluids have been discussed although several studies on the nanofluid flow phenomena are presented with various conditions.
- Investigation on the role of thermal radiation and dissipative heat is not new to the studies but the influence of these factors with the involvement of space and time-dependent heat source/sink over the Riga plate is conducted in this study.
- The impact of permeability on the transport characteristics of nanofluids over time required detailed investigation.
- The application of numerical technique i.e. spectral quasilinearization method for the system is rare.

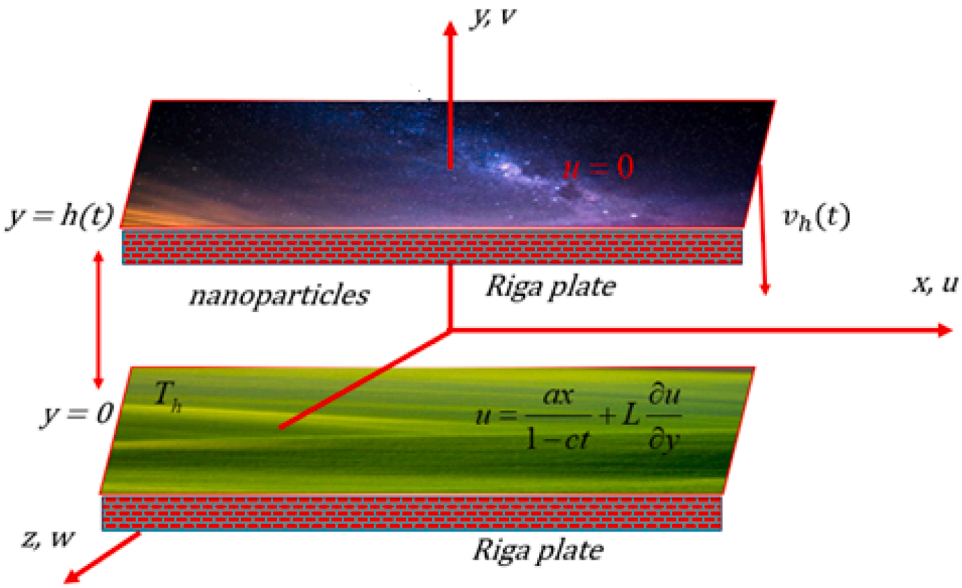

Fig. 1. Flow configuration defining the Cu∼water/Cu∼kerosene nanofluids within parallel Riga plates embedding with a porous matrix where the convective thermal condition is assumed along with thermal radiation, dissipative heat, and heat source/sink.

Primitive goal of the investigation: The major goal of the current investigation is to deploy a comparative analysis of water/kerosene-based Cu nanofluid under time-dependent radiative flow between squeezing Riga plates. Incorporating non-uniform heat source/sink and thermal convective boundary conditions in a permeable medium. The study aims to assess the influence of these factors on heat dissipation and flow characteristics, using the spectral quasilinearization method for precise numerical solutions.

Novel approach to the investigation

- A comparative study is presented for the consideration of Cu∼water and Cu∼kerosene nanofluids through parallel Riga plates embedding within a porous matrix.
- Interaction of non-uniform heat source/sink into a time-dependent nanofluid flow model shows a more realistic simulation for the heat transport phenomena of industrial processes.
- Potential advancement in thermal management applications is explored for the impact of dissipative heat along with thermal radiation over a Riga surface.
- Utilization of SQLM in solving the time-dependent nonlinear flow model of nanofluid provides computational efficiency in predicting heat transfer rates.

The proposed Darcy's law is known as linear and it is applicable to slow, laminar flows past permeable medium. However, increasing the velocity of the flow there is a significant effect of inertia occurs and this lead to the inclusion of nonlinear Forchheimer term. Further, the Forchheimer effects are more pronounced in low permeability and porosity of the medium. There is an increase in the resistance with the decrease of pore size, making the inertial losses described by the Forchheimer term more significant in this study.

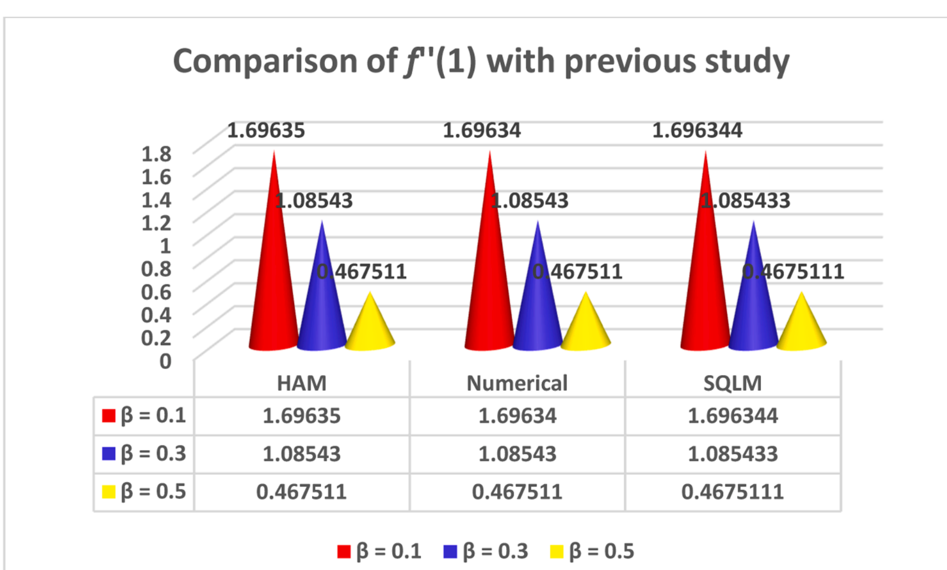

Fig. 2. Comparison with previous study (Hayat et al.[23]) at Ec, Da, $\phi = 0$.

2. Mathematical formulation

Flow of nanofluid comprised of Cu as a nanoparticle dispersed into water/kerosene is presented that provides a comparative analysis between two distinct nanofluid in various physical situations. The flow occurs within two parallel Riga plates suggests a squeezing flow, placed at a distance $h(t) = (a/v_f(1-\gamma t))^{-1/2}$with the interaction of permeable medium. The assumption shows that, the lower plate is kept at $y = 0$ i.e., towards the positive x-direction whereas the upper is located at$y = h(t)$. Here, a, indicates the rate constant and $t$is used as time-varying parameter. The plate velocity at the lower surface is presumed as$U_w = ax/(1-\gamma t)$. The suction velocity at the upper Riga surface is also time-varying and denoted as $vh = dh/dt$ (Fig. 1) In an advance, the role of Darcy dissipation cannot be neglected due to the interaction of permeability of the medium and along with the impact of thermal radiation with space and temperature-dependent heat source/sink is considered (Fig. 2).

Considering above assumptions, the model problem is described as (Hayat et al. ,[23] Ali et al.[27]),

$$\left(\frac{\partial}{\partial x}\hat{i}+\frac{\partial}{\partial y}\hat{j}\right).(u\hat{i}+v\hat{j}) = 0 \tag{1}$$

$$\rho_{nf}\frac{D}{Dt}u = -\frac{\partial p}{\partial x}+\mu_{nf}\left(\frac{\partial^2 u}{\partial x^2}+\frac{\partial^2 u}{\partial y^2}\right)-\frac{\mu_{nf}}{k_p^*}u+\frac{1}{8}\pi j_0 M_0 Exp\left(-\frac{\pi}{b}y\right) \tag{2}$$

$$\rho_{nf}\frac{D}{Dt}v = -\frac{\partial p}{\partial y}+\mu_{nf}\left(\frac{\partial^2 v}{\partial x^2}+\frac{\partial^2 v}{\partial y^2}\right) \tag{3}$$

$$(\rho Cp)_{nf}\frac{D}{Dt}T = \kappa_{nf}\left(\frac{\partial^2 T}{\partial x^2}+\frac{\partial^2 T}{\partial y^2}\right)+\mu_{nf}\left(4\left(\frac{\partial u}{\partial x}\right)^2+\left(\frac{\partial v}{\partial x}+\frac{\partial u}{\partial y}\right)^2\right) + \frac{16\sigma^* T_m^3}{3k^*}\frac{\partial^2 T}{\partial y^2}+\frac{\mu_{nf}}{k_p^*}u^2+Q''' \tag{4}$$

$$\left.\begin{aligned} &u = U_w + L\frac{\partial u}{\partial y} = \frac{ax}{1-ct}+L\frac{\partial u}{\partial y}, v = 0, -k_{nf}\frac{\partial T}{\partial y} = \hbar(T_h - T) \quad at \quad y = 0,\\ &u = 0,\ v = v_h = \frac{dh}{dt} = -\frac{c}{2}\sqrt{\frac{nu}{a(1-ct)}}, T = T_h \quad at \quad y = h(t) \end{aligned}\right\} \tag{5}$$

In particular, the operator $\frac{D}{Dt}(\bullet) = \frac{\partial}{\partial t}(\bullet)+u\frac{\partial}{\partial x}(\bullet)+v\frac{\partial}{\partial y}(\bullet)$

In general sense the Cartesian coordinate system is expressed by considering the main flow axis as x and y which is normal to it with velocity components$u$, and $v$respectively. The current density, $j_0(A/m^2)$, applied in the electrodes, magnetization, M_0(Tesla), where, b, width of magnets and electrodes. Furthermore, $T$and T_0represented as temperature of fluid and solid surface respectively, with dimensionless constants $a$andγ.

The viscosity is used in the governing equation for the two distinct nanofluids such as water-based Cu / kerosene-based Cu and the thermophysical properties are also mentioned. The thermophysical properties of each of the factors i.e., viscosity, thermal conductivity, density are the function of volume fraction which enhances the entire flow phenomena particularly the heat transport phenomenon. This is due to the fact that the thermal conductivity of the nanofluid in each of the case is enhanced in comparison to the base liquid water/kerosene.

The standard physical properties used for the properties of nanofluid are: (Batchelor et al. ,[28] Mintsa et al.[29])

$$\left.\begin{aligned} &A_1 = \frac{\mu_{nf}}{\mu_f} = (1+2.5\phi+6.25\phi^2), A_2 = \frac{\rho_{nf}}{\rho_f} = 1-\phi+\frac{\rho_s}{\rho_f}, A_3 = \frac{k_{nf}}{k_f} = (1+1.72\phi)\\ &A_4 = \frac{(\rho C_p)_{nf}}{(\rho C_p)_f} = (1-\phi)+\phi\frac{(\rho C_p)_s}{(\rho C_p)_f}, \alpha_{nf} = \frac{k_{nf}}{(\rho C_p)_{nf}} \end{aligned}\right\} \tag{6}$$

Following transformations are utilized in converting the dimensionless form of the governing equation and these are:

$$\left.\begin{aligned} &\psi = \sqrt{\frac{av_f}{1-ct}}xf(\eta), \eta = \frac{y}{h(t)}, u = U_w f'(\eta), v = -\sqrt{\frac{av_f}{1-ct}}f(\eta),\\ &w = U_w g(\eta), \theta(\eta) = \frac{T-T_m}{T_h-T_m}, U_w = \frac{ax}{(1-ct)} \end{aligned}\right\} \tag{7}$$

Implementing the similarity variables in Eqs (2)-(4)

$$\frac{A_1}{A_2}f^{iv}-\left(f f''-ff'''+\frac{\beta}{2}(3f''+\eta f''')\right)-\frac{A_1}{A_2}Daf''-\frac{Q}{A_2}\mathrm{H}\exp(-\eta H) = 0 \tag{8}$$

$$\frac{1}{A_4 \Pr}(A_3+Nr)\theta''+\Pr(A^* f'+B^*\theta)+\frac{A_1}{A_4}EcDaf'^2+f\theta'-\frac{\eta\beta\theta'}{2} + EcA_1(4\delta^2 f'^2+f''^2) = 0 \tag{9}$$

With

$$\left.\begin{aligned} &f(0) = 0,\ f'(0) = 1+\lambda f''(0),\ A_3\theta'(0) = -Bi(1-\theta(0))\\ &f(1) = \frac{\beta}{2},\ f'(1) = 0,\ \theta(1) = 0, \end{aligned}\right\} \tag{10}$$

The non-dimensional parameters involved in the transformed equations are, Q is the modified Hartman number, Pr, the Prandtl number, β, the squeezing factor, Bi, the thermal convection, A^*, B^*, the space and temperature-dependent heat source/sink, with other characterizing factors are described as:

$$\left.\begin{aligned} &\Pr = \frac{\mu_f Cp}{k}, Me = \frac{(Cp)_f(T_h-T_m)}{\lambda+cs(T_m-T_0)}, \beta = \frac{c}{a}, Q = \frac{\pi_j M_0 x}{8\rho_f U_w^2},\\ &H = \frac{\pi}{b}, \delta = \sqrt{\frac{(1-ct)v_f}{ax}}, \omega = \frac{\Omega}{a}, Bi = -\frac{h_1}{k}\sqrt{\frac{v_f(1-ct)}{a}}, Nr = \frac{16\sigma^* T_m^3}{3k^* k_f} \end{aligned}\right\} \tag{11}$$

The engineering coefficients such as the skin friction coefficient Cf_x and local Nusselt number Nu_x are defined as follows:

$$C_{fx} = \frac{\tau_w}{\rho_f U_w^2}, Nu_x = \frac{xq_w}{k_f(T_h-T_m)}, \tag{12}$$

where the wall shear stress τ_w and the wall heat fluxq_w are

$$\tau_w = \mu_{nf}\left(\frac{\partial u}{\partial y}\right)_{y=0}, q_w = -k_{nf}\left(\frac{\partial T}{\partial y}\right)_{y=0}-(q_r)_{y=0} \tag{13}$$

The dimensionless quantities are:

$$Cf\mathrm{Re}_x^{1/2} = A_1 f''(0), Nu_x \mathrm{Re}_x^{1/2} = -(A_3+Nr)\theta'(0), \tag{14}$$

Where $\mathrm{Re}_x = \frac{U_w x}{v}$is the local Reynolds number.

3. Spectral quasilinearisation method

In this study, we apply an iterative method known as the "Spectral Quasi-linearisation Method (SQLM)" to numerically tackle a series of ordinary differential equations specified in equations (8 - 9), related to the boundary constraints defined in Eq. (10). This technique begins by linearizing the governing nonlinear equations through the "Newton-Raphson-based quasilinearisation method (QLM)", originally reported by Bellman and Kalaba[21] in 1965. Following this, the linearized

Table 1
Thermophysical properties of nanofluids.

	$\rho(kg/m^3)$	$k(W/mK)$	$Cp(J/kgK)$	Pr
Pure water	997.1	0.613	4179	6.2
Copper	8933	401	385	–
Kerosene oil	783	0.145	2090	21

equations are solved using the Chebyshev spectral collocation method. When compared to conventional numerical techniques like the "shooting method", "Runge-Kutta method", and "Keller Box method", the SQLM demonstrates enhanced stability, high computational accuracy and minimized computation time. The SQLM employs the Newton-Raphson method to linearize both nonlinear ODEs and PDEs. The process involves applying Taylor series expansion to the nonlinear components of the governing equations, assuming a small difference among the values of the unidentified function at the current iteration ($m + 1$) and the previous one (m). For a more detailed explanation of this method, refer to Motsa.[22] By implementing the QLM on the two nonlinear ordinary differential equations, which involve the unknown functions $f(\eta)$ and $\theta(\eta)$ as described in equations (8 - 9), the equations take the following form:

$$\alpha_{0,m} f^{iv}_{m+1} + \alpha_{1,m} f''_{m+1} + \alpha_{2,m} f'_{m+1} + \alpha_{3,m} f'_{m+1} + \alpha_{4,m} f_{m+1} = \Lambda_f, \tag{15}$$

$$\sigma_{0,m}\theta''_{m+1} + \sigma_{1,m}\theta'_{m+1} + \sigma_{2,m}\theta_{m+1} + \sigma_{3,m} f''_{m+1} + \alpha_{4,m} f'_{m+1} + \alpha_{5,m} f_{m+1} = \Lambda_\theta. \tag{16}$$

The variable coefficients $\alpha_{r,m}$ and $\sigma_{r,m}(where\ r = 1, 2, 3, \ldots)$ are defined as:

$$\alpha_{0,m} = \frac{A_1}{A_2}, \alpha_{1,m} = f_m - \frac{\beta}{2}\eta, \alpha_{2,m} = -f'_m - 3\frac{\beta}{2} - \frac{A_1}{A_2}Da, \alpha_{3,m} = -f''_m, \alpha_{4,m} = f'''_m,$$

$$\sigma_{0,m} = \frac{1}{A_4 Pr}(A_3 + Nr), \sigma_{1,m} = f_m - \frac{\beta}{2}\eta, \sigma_{2,m} = PrB^*, \sigma_{3,m} = 2f''_m EcA_1,$$

$$\sigma_{4,m} = PrA^* + \frac{A_1}{A_4}2f'_m EcDa + 8EcA_1\delta^2 f'_m, \sigma_{5,m} = \theta'_m. \tag{17}$$

The right-hand side of Eqs. (15 – 16) are defined as:

$$\Lambda_f = -f'_m f''_m + f_m f''_m + \frac{Q}{A_2}Hexp(-\eta H)$$

$$\Lambda_f = -f'_m f''_m + f_m f''_m + \frac{Q}{A_2}Hexp(-\eta H),$$

$$\Lambda_\theta = \frac{A_1}{A_4}EcDaf'^2_m + f_m\theta'_m + 4EcA_1\delta^2 f'^2_m + EcA_1 f''^2_m. \tag{18}$$

The iterative approach described in Eqs. (15–16) serves as the operational framework for the "spectral quasi-linearisation method", which is then, addressed using the "Chebyshev spectral collocation technique". By utilizing appropriate initial estimates, the iteration schemes (15–16) are solved in sequence to compute f_{m+1} and θ_{m+1}. The initial approximation required to initiate the SQLM algorithm are specified as follows:

$$f_0(\eta) = \left(\frac{-\beta + 1 - \lambda\beta}{1 + 4\lambda}\right)\eta^3 + \left(\frac{3\beta - 4}{2(1 + 4\lambda)}\right)\eta^2 + \left(\frac{1 + 3\lambda\beta}{1 + 4\lambda}\right)\eta, \theta_0(\eta) = \frac{B_i}{A_3}\eta(\eta - 1). \tag{19}$$

The Chebyshev spectral collocation method is employed to solve Eqs. (15)–(16) discretizing them within the computational interval $[-1, 1]$. Prior to employing this spectral technique, it is essential to transform the domain [0, 1] into the domain $[-1, 1]$. Furthermore, we introduce a differentiation matrix, referred to as $\boldsymbol{D}$, to calculate the derivatives of the unknown functions $f(\eta)$ and $\theta(\eta)$ at the designated collocation points. This transformation, represented as $\eta = (\zeta + 1)/2$, maps the interval [0, 1] onto $[-1, 1]$.

Table 2

Convergence and Residual Error for eqations (8–9) (Cu/Water), when $Da = 0.1$, $\lambda = 0.5$, $\beta = 0.1$, $Nr = 0.5$, $Pr = 6.2$, $Ec = 0.1$, $\delta = 0.5$, $Q = H = 1$, $\phi = 0.1$, $A^* = B^* = B_i = 0.1$.

iterations	$\|\|Res(f)\|\|_\infty$	$\|\|Res(\theta)\|\|_\infty$	E_f	E_θ
1	1.198×10^{-2}	8.166×10^{-3}	4.595×10^{-3}	1.433×10^{-1}
2	1.055×10^{-3}	6.276×10^{-6}	1.327×10^{-4}	4.213×10^{-2}
3	4.533×10^{-5}	2.353×10^{-9}	2.499×10^{-6}	2.121×10^{-5}
4	1.051×10^{-6}	8.072×10^{-13}	2.187×10^{-8}	2.447×10^{-7}
5	1.017×10^{-8}	7.330×10^{-14}	1.188×10^{-9}	3.771×10^{-9}
6	4.986×10^{-10}	3.786×10^{-14}	3.570×10^{-11}	4.206×10^{-11}
7	1.793×10^{-11}	1.649×10^{-14}	4.787×10^{-13}	3.621×10^{-12}
8	1.653×10^{-13}	2.762×10^{-14}	2.426×10^{-14}	1.621×10^{-13}
9	2.638×10^{-13}	6.256×10^{-14}	1.422×10^{-14}	2.820×10^{-14}
10	1.432×10^{-13}	1.483×10^{-14}	6.675×10^{-15}	9.148×10^{-14}

Table 3

Convergence and Residual Error for eqations (8 – 9) (Cu/Kerosine oil), when $Da = 0.1$, $\lambda = 0.5$, $\beta = 0.1$, $Nr = 0.5$, $Pr = 21$, $Ec = 0.1$, $\delta = 0.5$, $Q = H = 1$, $\phi = 0.1$, $A^* = B^* = B_i = 0.1$.

iterations	$\|\|Res(f)\|\|_\infty$	$\|\|Res(\theta)\|\|_\infty$	E_f	E_θ
1	1.581×10^{-2}	2.011×10^{-2}	6.412×10^{-3}	8.407×10^{-1}
2	1.667×10^{-3}	6.703×10^{-6}	2.039×10^{-4}	8.105×10^{-3}
3	8.731×10^{-5}	8.608×10^{-9}	4.701×10^{-6}	5.744×10^{-5}
4	2.465×10^{-6}	4.401×10^{-12}	4.984×10^{-8}	4.291×10^{-7}
5	3.064×10^{-8}	2.391×10^{-14}	3.538×10^{-9}	5.692×10^{-8}
6	1.868×10^{-9}	3.093×10^{-14}	1.282×10^{-10}	1.658×10^{-9}
7	8.207×10^{-11}	2.645×10^{-14}	2.075×10^{-12}	8.529×10^{-12}
8	1.053×10^{-13}	4.326×10^{-14}	6.552×10^{-14}	1.408×10^{-12}
9	4.717×10^{-13}	2.516×10^{-14}	2.219×10^{-14}	1.031×10^{-13}
10	7.581×10^{-14}	2.534×10^{-14}	3.553×10^{-14}	2.376×10^{-14}

The SQLM method for Eqs. (15)–(16) can be represented in matrix form as:

$$\begin{bmatrix}\Delta_{11} & \Delta_{12}\\ \Delta_{21} & \Delta_{22}\end{bmatrix}\begin{bmatrix}f_{m+1}\\ \theta_{m+1}\end{bmatrix} = \begin{bmatrix}\Lambda_1\\ \Lambda_2\end{bmatrix},$$

where

$$\Delta_{11} = [\alpha_{0,m}]\boldsymbol{D}^4 + diag[a_{1,m}]\boldsymbol{D}^3 + diag[a_{2,m}]\boldsymbol{D}^2 + diag[a_{3,m}]\boldsymbol{D} + diag[a_{4,m}],$$

$$\Delta_{12} = 0,$$

$$\Delta_{21} = diag[\sigma_{3,m}]\boldsymbol{D}^2 + diag[\sigma_{4,m}]\boldsymbol{D} + diag[\sigma_{5,m}],$$

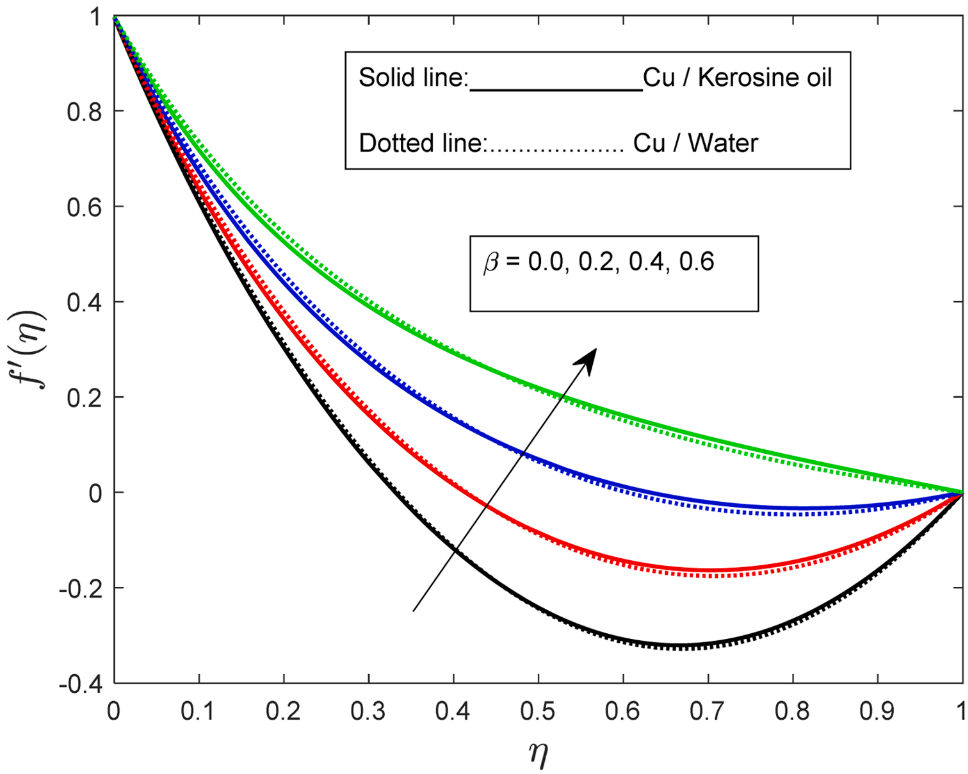

Fig. 3. Influence of βon $f'(\eta)$.

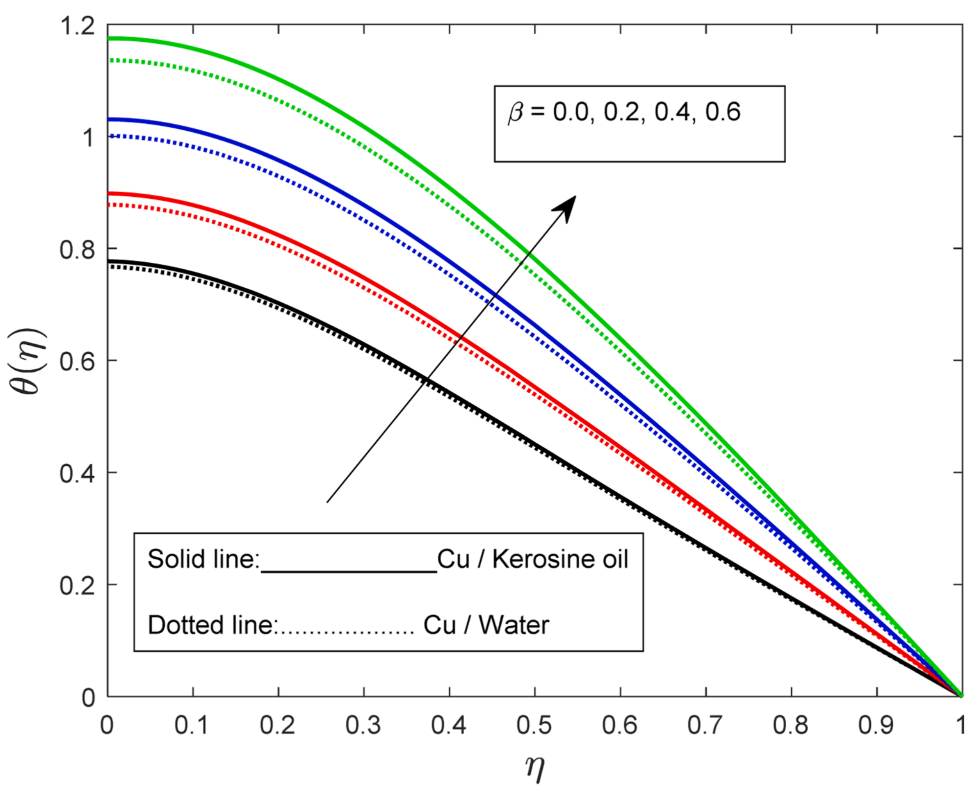

Fig. 4. Influence of β on θ(η).

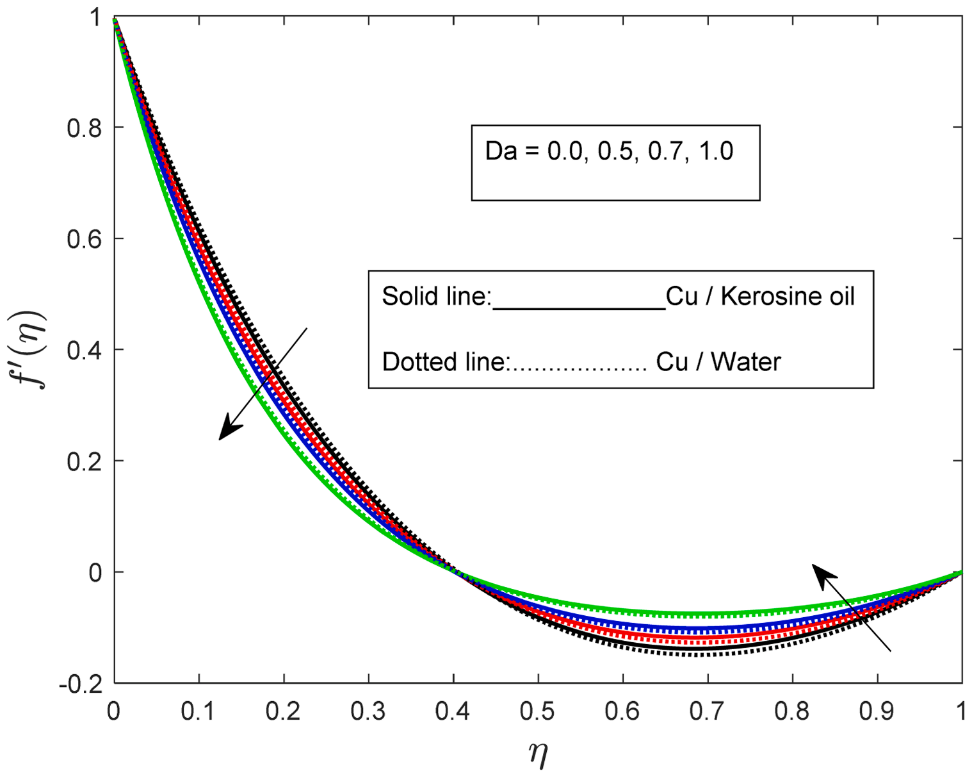

Fig. 5. Influence of *Da*on $f'(\eta)$.

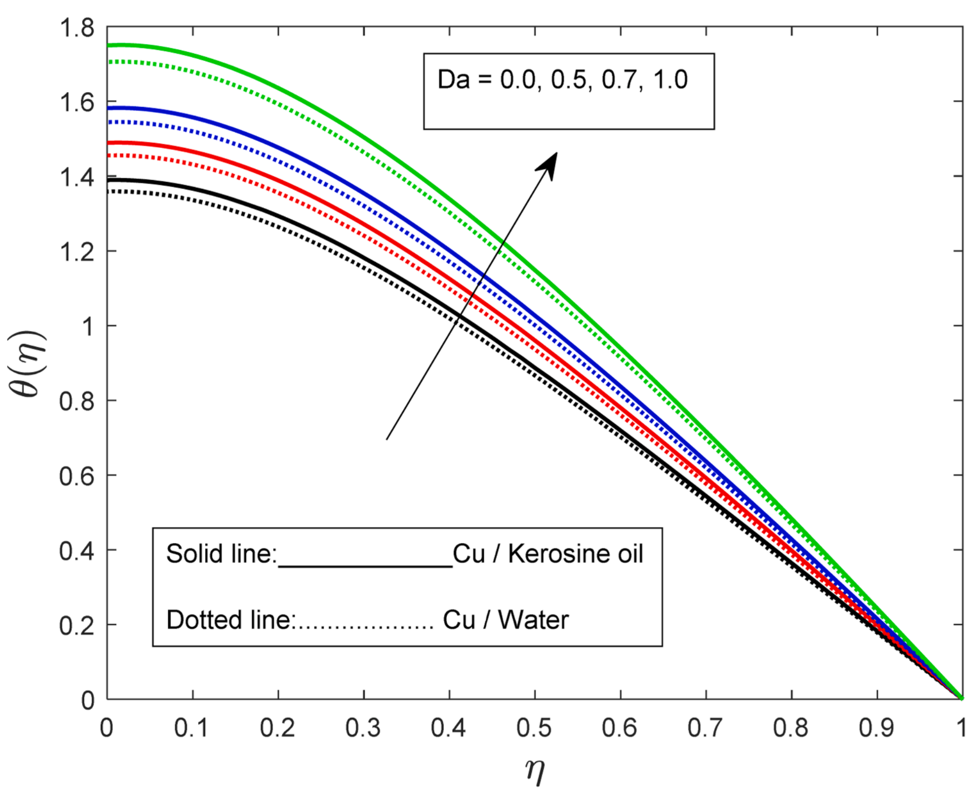

Fig. 6. Influence of *Da*on $\theta(\eta)$.

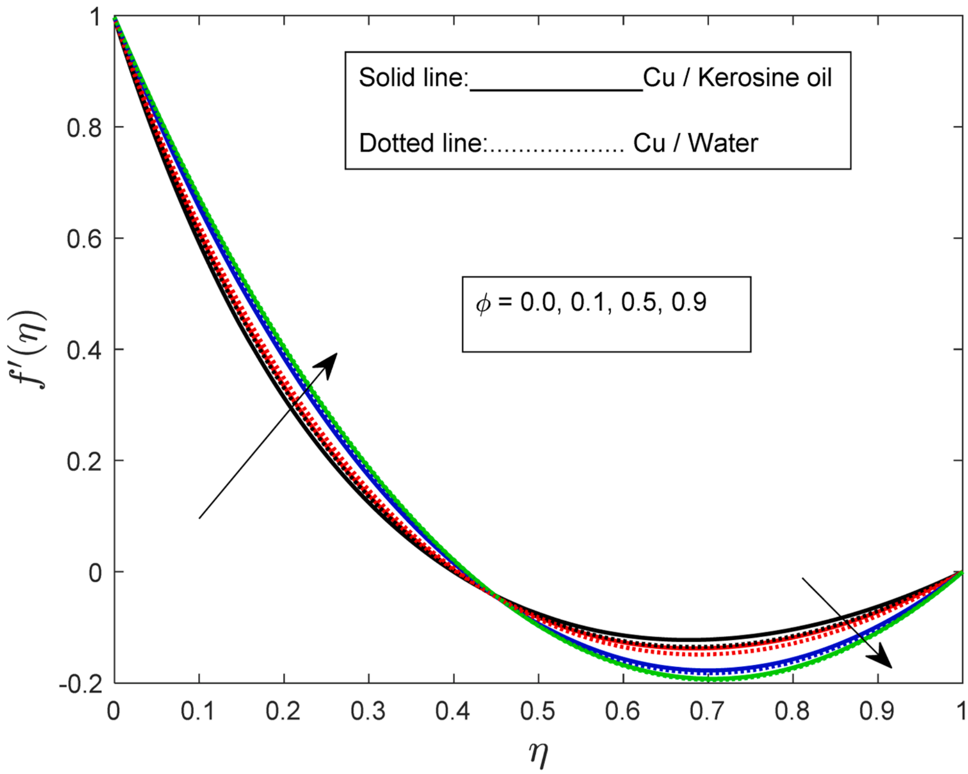

Fig. 7. Influence of ϕon $f'(\eta)$.

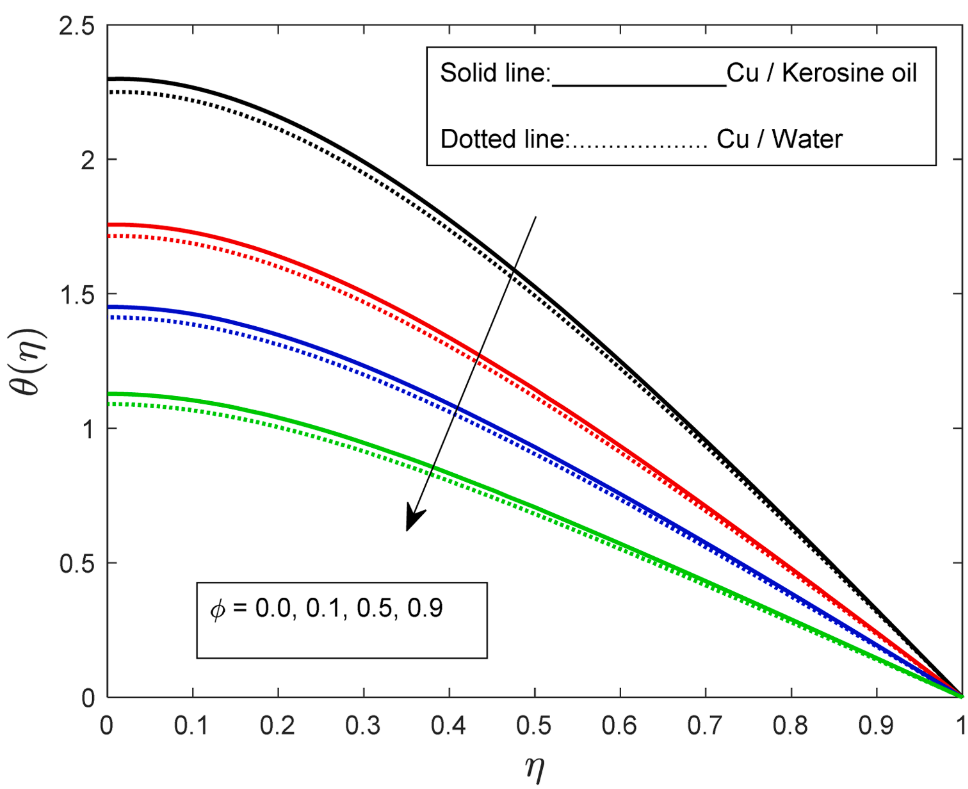

Fig. 8. Influence of ϕon θ(η).

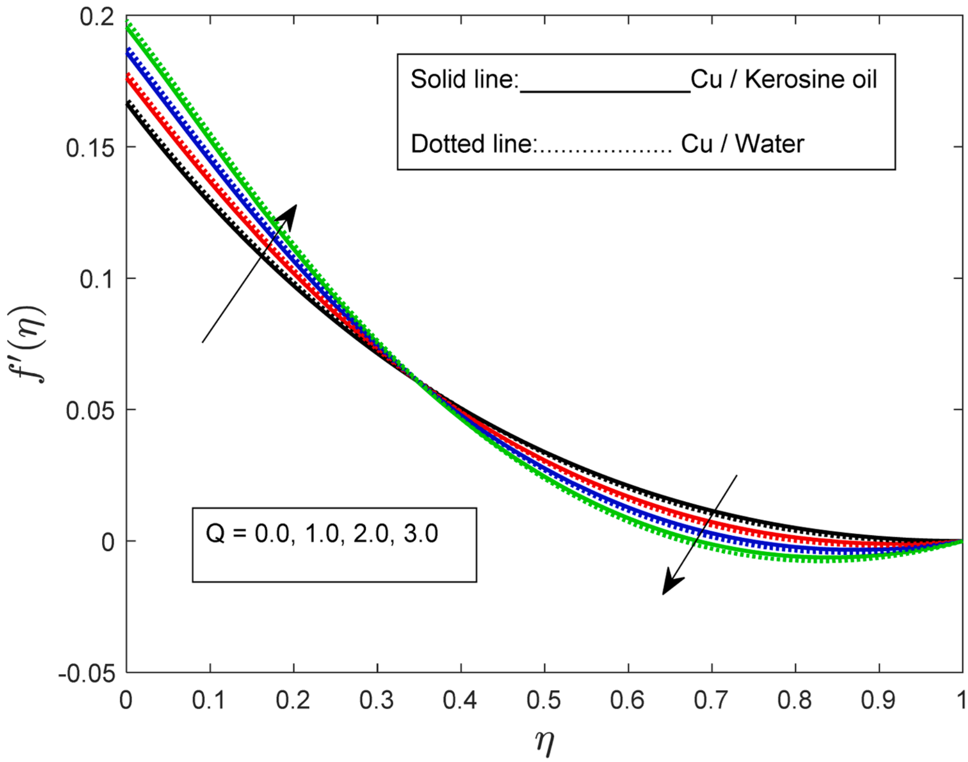

Fig. 9. Influence of Q on $f'(\eta)$.

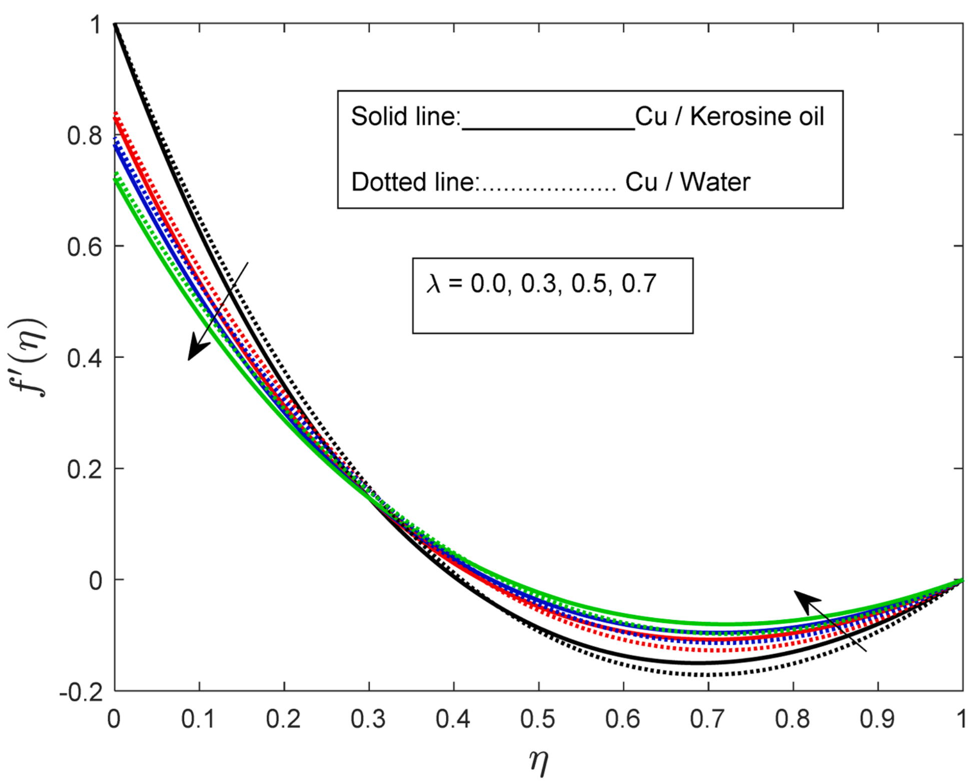

Fig. 10. Influence of λ on $f'(\eta)$.

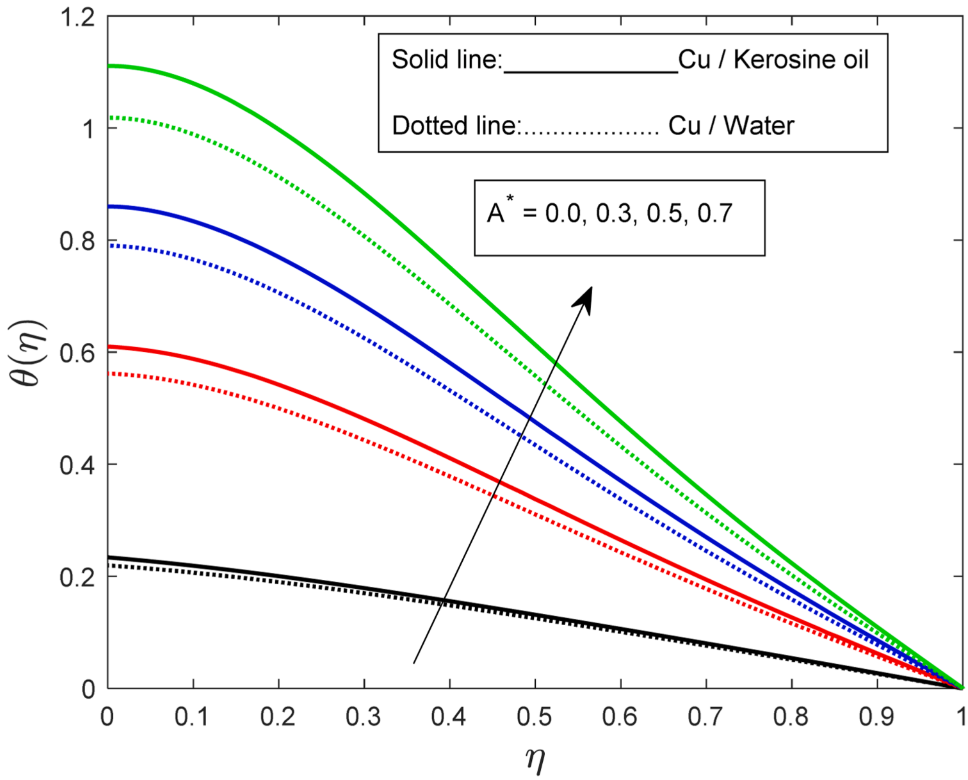

Fig. 11. Influence of A^* on θ(η).

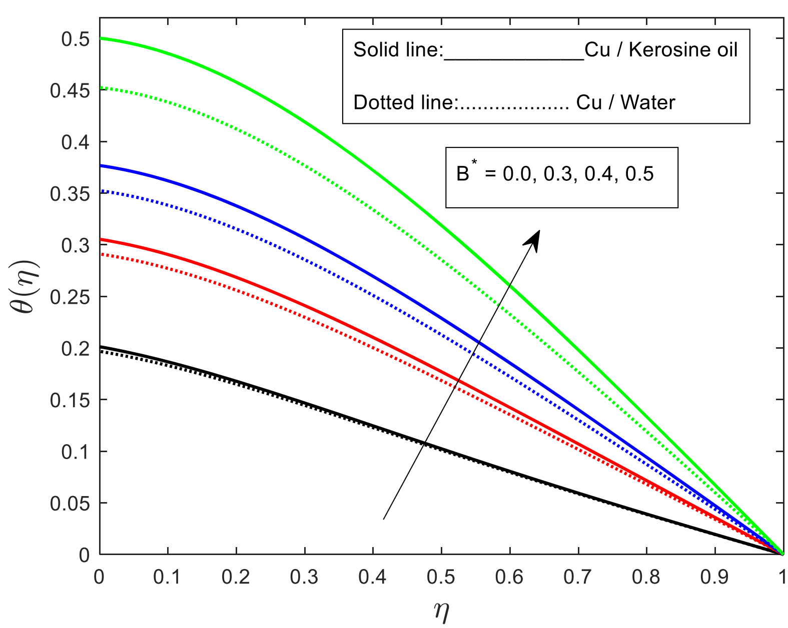

Fig. 12. Influence of B^* on θ(η).

$\Delta_{22} = \sigma_{0,m}\boldsymbol{D}^2 + \ diag[\sigma_{1,m}]\boldsymbol{D} + \ \sigma_{2,m}\boldsymbol{I}.$

In the notation presented above, "*diag*" is a diagonal matrix of size $(N_x + 1) \times (N_x + 1)$ "$\boldsymbol{I}$" denotes an identity matrix sized $(N_x + 1) \times (N_x + 1)$, and "$\boldsymbol{D}$" shows differentiation with respect to ζ and "N_x" is the number of collocation points.

4. Results and discussion

In this study, we employ the "Spectral Quasi-linearisation Method" to perform numerical simulations for the nonlinear coupled system of ODEs modeling the fluid flow under consideration. Table 1 represents the thermal attributes of the solid nanoparticles as well as the base liquid water/kerosene. The results obtained are compared with existing literature (Hayat et al.[23]) to validate our findings. Various dimensionless variables on the velocity and temperature profiles and other key material properties were analyzed and evaluated. For accurate and convergent results, appropriate initial guess functions and a range of physical parameter values are carefully selected and adjusted as necessary. The

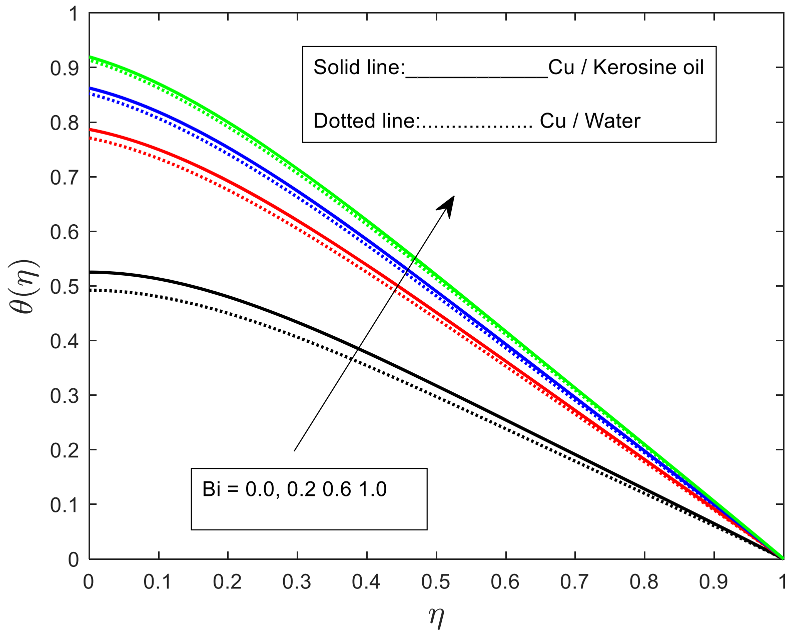

Fig. 13. Influence of *Bi* on θ(η).

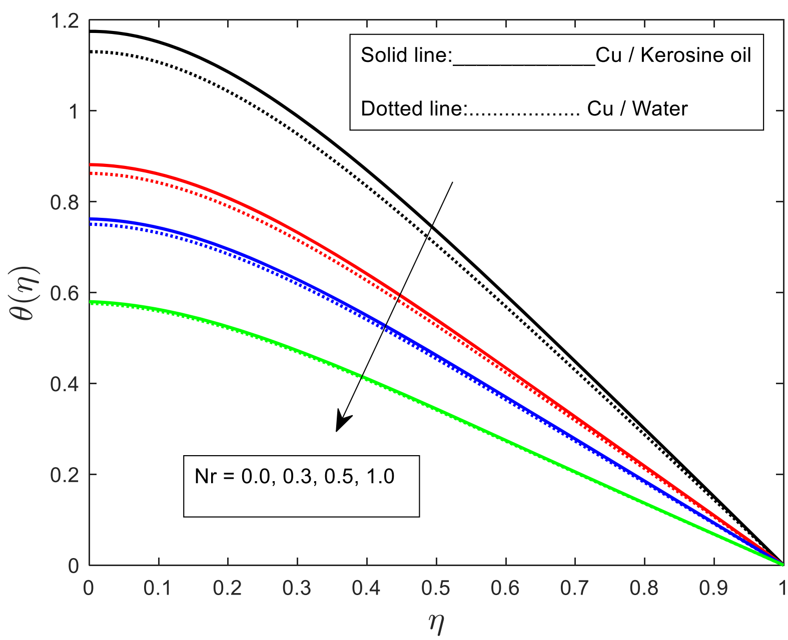

Fig. 14. Influence of *Nr* on θ(η).

SQLM results were generated using MATLAB. To demonstrate the convergence of the SQLM, solution errors are examined. This solution error is defined as the differences between the approximated function values across iterations. Convergence is illustrated using the infinity norm as seen in Table 2, which shows a steady decline in convergence errors as the number of iterations increases, confirming the accuracy of the numerical scheme. In addition, the accuracy of the solution method was evaluated by analyzing the residual errors of the functions after a set number of iterations. This process involved substituting the approximate solutions into the differential Eqs. (8–9) and computing the infinity norm of the residual error, as detailed in Tables 2 and 3 respectively. The Tables illustrate the behavior of residual errors $||Res(f)||_\infty$ and $||Res(\theta)||_\infty$ solution error norms E_f and E_θ against the number of iterations for both Cu/Water and Cu/Kerosine oil. The results confirm the convergence and accuracy of the numerical scheme, as indicated by a steady decrease in both residual errors and solution error norms with increasing iterations. convergence is achieved after relatively few iterations. It is also notable that the error estimates for the SQLM are consistently lower, demonstrating that the SQLM is convergent and accurate.

The behaviour of several factors affecting the flow phenomena are depicted through graphs and the results are obtained considering these values of the parameters within their specified domain. Further, the comparative analysis is deployed for the Cu∼water and Cu∼kerosene nanofluids in each of the profiles. Figs. 3 and 4 depict the significant role of the squeezing parameter on the fluid velocity and temperature distribution respectively. The distribution of the squeezing factor, β is demonstrated considering the numerical values as β = 0, 0.2, 0.4 and

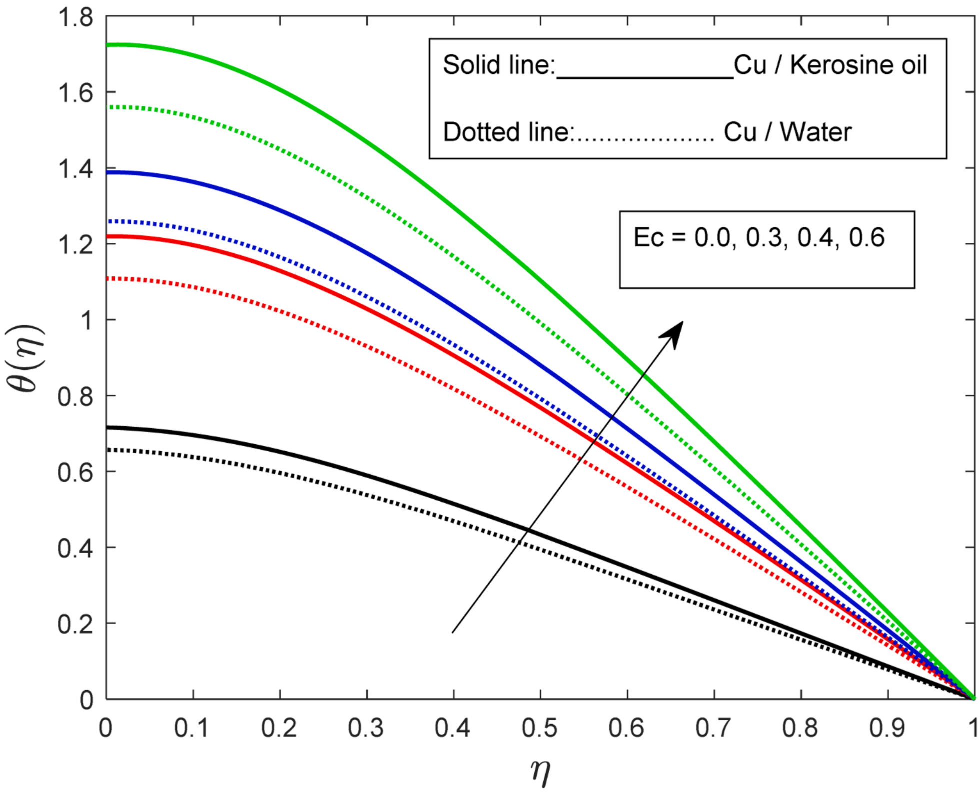

Fig. 15. Influence of *Ec* on θ(η).

0.6. The assigned numerical value $\beta = 0$signifies there is no squeezing effect. Further, in this case the velocity distribution shows its minimum impact near the surface region. The positive values of the squeezing means the plates are separated from each other. Therefore, with increasing separation the fluid velocity increases significantly and the profiles are close towards the central region. For higher $\beta$the profile is more pronounced near the central region as compared to the lower variation. However, for the no squeezing effect the fluid temperature has less impact and the profile lower down towards the lower plate. With enhanced squeezing effect the fluid temperature increases more rapidly leading to a smaller flow domain and higher heat generation. The Cu~water nanofluid shows better temperature control compared to Cu~kerosene due to its higher heat transfer properties. The fact is clear from the depicted numerical tabular results that water has a higher thermal conductivity compared to kerosene and this suggests water can transfer more heat efficiently than keroisene, leading to better temperature regulation. Further, the viscosity of the water is low than that of kerosene allows for bettwer fluid flow and lead to higher velocity profiles. Finally, it is concluded that, Cu-water nanofluid exhibits better velocity as well as temperature performance as squeezing increases. The flow remains stable and temperature rises due to superior thermal properties of water.

Figs. 5 and 6 describes the impact of porosity on the velocity and temperature distribution of the nanofluids. The permeability of the medium is presented for the consideration of the factor porosity with their range as $Da \in [0, 1]$.Here, $Da = 0$signifies the flow through clear fluid and the non-zero values portrays the characteristic when the flow through permeable medium. The velocity distribution shows dual effect for the variation of the porosity. For the non-occurrence of the porous matrix, the appearance of lower resistive force augments the fluid velocity up to the center of the channel and for the increasing porosity, the resistivity increases which favors in decelerating the velocity profile and the profile is close to the lower plate of the channel. Moreover, the effect is reversed from the central region of the channel toward the upper plate. The impact of Cu-water nanofluid exhibits a greater role than that of Cu-kerosene nanofluid within the center of the channel. The resistivity of the permeability that favors reducing the fluid velocity generates energy at the lower surface of the plate. The stored energy boosts up and moves toward the upper plate. This causes a significant enhancement in the fluid temperature. The enhanced thermal properties of the cu nanoparticle in both of the base fluids became significant which overshoots the fluid temperature. The comparative analysis reveals that Cu water has a greater control in the fluid temperature than the kerosene-based nanofluid.

Particle concentrations generally known as the volume concentration of the nanoparticles have important applications on the nanofluid flow behaviour. Since each of the thermal properties is the function of volume concentration and these thermal properties are equipped with the flow and heat transfer phenomena of the proposed problem. Figs. 7 and 8 portray the characteristics of the concentration of the nanoparticle affecting the fluid velocity and the temperature of the nanofluid respectively. The variation is depicted considering the volume fraction as 0 % to 0.9 %. Here, 0 % volume fraction means the behaviour is presented for the pure fluid, water/kerosene. However, the variation of nanoparticles is considered for both the Cu-water and Cu-kerosene nanofluids. In the case of pure fluid the profile of velocity ceases its lower velocity at the lower plate of the channel and with increasing concentration, the fluid velocity enhances significantly. The enhanced concentration increases the density of the nanoparticles and the agglomeration of the particles is obtained near the lower surface. However, the opposite impact is rendered from the central region toward the upper plate region. The increasing concentration of the solid particle enhances the fluid temperature significantly. The segregation of the particles at the bottom of the surface and the enhanced conductivity of the nanoparticles enrich the fluid temperature at all points within the domain. The comparative results obtained between the Cu-water and Cu-kerosene show that the water-based nanofluid has greater control over the kerosene-based nanofluid. This fact is rendered due to the

Table 4

Computational values of $Re_x^{\frac{1}{2}}C_f$ for different values of β, λ, Da, Q, ϕ, H, when $Bi = 0.1$, $A^* = 0.1$, $B^* = 0.1$, $\delta = 0.3$, $Nr = 1$, $Ec = 0.1$, $Pr = 6.2$.

β	λ	Da	Q	H	ϕ	$Re_x^{\frac{1}{2}}C_f$ **Cu / Water**	$Re_x^{\frac{1}{2}}C_f$ **Cu / Kerosine oil**
0.1	0.3	0.1	1.5	10	0.1	− 2.3033140	−2.3322613
0.2						−2.1749495	−2.2122675
0.3						− 2.0379272	− 2.0810816
0.2	0.1	0.1	1.5	10	0.1	−3.6585787	− 3.7696517
	0.2					− 2.7238274	− 2.7831463
	0.5					− 1.5538929	− 1.5730007
0.2	0.3	0.1	1.5	10	0.1	−2.1749495	− 2.2122675
		0.2				− 2.1775750	− 2.2147000
		0.3				− 2.1801874	− 2.2171210
0.2	0.3	0.1	0.5	10	0.1	− 2.2000520	− 2.2364640
			1.0			− 2.1874969	− 2.2243614
			1.5			−2.1749495	− 2.2122675
0.2	0.3	0.1	1.5	3.0	0.1	− 2.1622116	− 2.2001009
				5.0		− 2.1632147	− 2.2010434
				7.0		− 2.1679166	− 2.2055374
0.2	0.3	0.1	1.5	10	0.05	− 1.9060514	− 1.9415571
					0.2	− 2.8569174	− 2.8975905
					0.3	− 3.7308755	− 3.7743135

higher thermal conductivity of the water in comparison to the kerosene.

The variation of Hartmann number along with velocity slip on the fluid velocity is presented in Figs. 9 and 10 respectively. Hartmann number variation is deployed considering the range of the parameter as $Q = 0, 1, 2, 3$.The numerical result of $Q = 0$signifies the no interaction of the magnetic field and the resistivity of the magnetization is presented through the non-zero values of the Hartmann number. The inclusion of the magnetization act as a drag effect on the fluid motion and the enhanced Hartmann number retards the fluid velocity at the upper plate surface. A dual characteristic is rendered for the variation of the Hartmann number and it is seen that with increasing Hartmann number the fluid velocity significantly enhances near the lower plate surface. In the proposed investigation, Cu-water nanofluid experiences a more significant reduction in velocity because of the higher electrical conductivity compared to the kerosene-based nanofluid. The variation of slip occurs considering the range of the parameter as $L \in [0, 0.7]$.Here, $L = 0$shows that the fluid velocity at the surface and the plate velocity are the same or both are constant. Furthermore, slip occurs when both the velocities differ from each other. The velocity profile shows dual impact within the channel and it is seen that for the increasing slip, the fluid velocity moves toward the lower plate causing a significant retardation in the velocity distribution but the reverse impact is observed at the upper plate. A similar impact is projected for the water/kerosene-based nanofluid. However, the comparative result reveals that the Cu-kerosene shows slightly higher velocity due to lower viscosity.

For a comparative study of space and temperature-dependent heat sources on the temperature profile of nanofluids, the variation of both the parameters are presented in Figs. 11 and 12 respectively. The behavior of the space-dependent parameter is depicted considering the numerical values as $A^* \in [0, 0.7]$and temperature-dependent parameter B^*as $B^* \in [0 - 1]$.The thermal conductivity of the Cu nanofluid is higher than that of the kerosene-based nanofluid which leads to faster heat conduction and smoother temperature gradient. In both A^* and B^* variations, the temperature profile show a greater rise due to better conduction properties. Further, lower conductivity of kerosene based nanofluid exhibits slower heat transfer and sharper temperature gradient. For the smaller values of A^*, both nanofluid experiences lower influence near the lower plate and further the increasing variation enhances the profile significantly. The similar observation is also rendered for the temperature dependent heat source for both the nanofluids.

The thermal Biot number is presented as the ratio of the conductive heat resistance to the convective heat transfer resistance at the solid-liquid interface. The no-dimensional parameter plays an important role in determining the temperature gradient within the system. Fig. 13 exhibits the variation of thermal Biot number on the temperature distribution of the nanofluids. The variation is deployed considering their range as $Bi \in [0, 1]$.Cu-water has higher conductivity compared to kerosene, as a result, the Cu-water shows faster heat transfer within the solid-liquid interface. The low $Bi(Bi = 0)$, indicates that conduction within the solid dominates and the temperature profile became flat at the interface. However, increasing Bi, the convective heat transfer became significant which resulted in a significant enhancement in the fluid temperature throughout. Due to high thermal conductivity of water, the Cu-water nanofluid exhibits a smoother temperature with more uniform heat distribution at higher Biot number.

A significant analysis of the thermal radiation on the temperature distribution of the nanofluids is displayed in Fig. 14. The variation of the

Table 5

Computational values of $Re_x^{\frac{1}{2}}Nu_x$ for different values of β, Bi, δ, A^*, B^*, ϕ, Ec, Da, when $Nr = 0.5$, $\lambda = 0.3$, $Q = 1.5$, $H = 10$.

β	Bi	δ	B^*	A^*	Ec	Da	ϕ	$Re_x^{1/2}Nu_x$ **Cu/Water**	$Re_x^{1/2}Nu_x$ **Cu/Kerosine oil**
0.1	0.1	0.3	0.1	0.1	0.1	0.1	0.1	0.3933449	0.3025334
0.3								0.3309756	0.2696656
0.5								0.2684469	0.2385837
0.2	0.1	0.3	0.1	0.1	0.1	0.1	0.1	0.3619051	0.2856221
	0.2							0.7603572	0.5831222
	0.3							1.2011868	0.8932569
0.2	0.1	0.2	0.1	0.1	0.1	0.1	0.1	0.3611926	0.2851992
		0.3						0.3619051	0.2856221
		0.5						0.3641851	0.2869753
0.2	0.1	0.3	0.1	0.1	0.1	0.1	0.1	0.3619051	0.2856221
			0.3					0.1602996	0.1653643
			0.6					0.1407383	0.1479401
0.2	0.1	0.3	0.1	0.1	0.1	0.1	0.1	0.3619051	0.2856221
				0.2				0.5399000	0.3980261
				0.3				0.7178949	0.5104300
0.2	0.1	0.3	0.1	0.1	0.2	0.1	0.1	0.4132388	0.3186561
					0.3			0.4645725	0.3516901
					0.5			0.5672400	0.4177581
0.2	0.1	0.3	0.1	0.1	0.1	0.2	0.1	0.3615407	0.2853724
						0.3		0.3611783	0.2851240
						0.5		0.3604595	0.2846315
0.2	0.1	0.3	0.1	0.1	0.1	0.1	0.02	0.3312170	0.2913703
							0.05	0.3184263	0.2885822
							0.07	0.3065361	0.2871692

factor Nr is presented within the range of $Nr \in [0, 1]$.In case of Cu-water, for the low $Nr(Nr = 0)$, a minimal thermal radiation, the heat transfer is dominated by conduction and convection. As thermal radiation increases, the heat transfer became significant and the profile temperature increase at the upper plate of the channel. Therefore, it radiates temperature towards the cooler region i.e. toward the lower plate. In case of Cu-kerosene, as thermal radiation increases, the temperature profile became significant due to the lower specific heat of kerosene. The radiation amplifies the temperature profile and Cu nanoparticle further boost thermal conductivity leading to more significant heat transfer in comparison to water based nanofluid.

Eckert number is one of the significant factors which is expressed as the ratio of the kinetic energy to enthalpy which affects the fluid temperature of the nanofluids. Fig. 15 characterizes the impact of Eckert number on the fluid temperature which is exhibited due to the interaction of dissipative heat impact, The variation of the proposed factor is presented within the range of $Ec \in [0, 0.6]$.In the absence of Ec, the kinetic energy became minimal and viscous dissipation is negligible. As a result, the profile depends upon the heat conduction only. With increasing Ec, viscous dissipation starts to contribute more significantly to heat generation and in the case of Cu-water nanofluid, known for higher thermal conductivity the temperature profile shows an increasing gradient, indicating enhanced energy transfer. Again, for Cu-kerosene nanofluid, the lower specific heat and thermal conductivity of kerosene result in a sharper temperature gradient compared to water. Therefore, Cu-water with higher thermal conductivity exhibits more uniform temperature throughout the domain.

The simulations are obtained for the engineering coefficients like shear rate and heat transfer rate for the variation of different physical quantities. The observation shows the computation of water/kerosene-based copper nanofluid separately. Table 4 displays the shear rate analysis for diversified characterizing factors. It is noteworthy that the increase in squeezing parameter occurs due to the separation of plates along with the increase in velocity slip favors in controlling the shear rate. This deceleration is exhibited for the consideration of both fluids. Further, in comparison to both cases, it is clear to observe that the case of water-based nanofluid has less prominence than that of kerosene and the fact is due to the higher density of the water. Again, the resistivity due to the permeability of the medium gives rise to an enhance the shear rate throughout but the modified Hartmann number attenuates it significantly. An enhanced concentration of the nanoparticle provides a greater strength in the rate coefficient and the comparative analysis shows that water-based has greater control than that of kerosene-based nanofluid.

In a similar approach, the heat transfer rate for the variation of characterizing factors is depicted in Table 5 and the results are presented for both the water/kerosene nanofluids. The enhanced squeezing factor has a greater role in attenuation in the heat transfer rate at the surface. However the convective heat transfer condition leads to showing the impact of the Biot number accelerating the rate coefficients throughout, The temperature-dependent heat source favors controlling the heat transfer rate but the space-dependent heat source has a reverse impact on the rate profiles. The coupling effect due to the increase of the Eckert number retards the profile of the heat transfer rate coefficients. However, porosity has an insignificant contribution but a slight deceleration in the heat transfer rate is observed for the increasing porosity. The nanoparticle concentration always favors control the heat transfer rate throughout the domain but the comparison between the water and kerosene shows that water is more prominent than kerosene in enhancing the heat transfer rate within the domain.

Conclusive remark

The forced convection of time-dependent nanofluids utilizing both water/kerosene between the parallel Riga plate embedding within the medium. The impact of dissipative heat along with thermal radiation and the non-uniform heat source enriches the flow profile. Further, investigation is carried out for the inclusion of velocity slip and thermal convection conditions. The spectral quasilinearization method is employed for the proposed model and the behavior of various factors is exhibited. However, the important outcomes are;

- The comparative as well as the convergence analysis with earlier investigation is presented which shows a good correlation.
- A drastic change in the fluid velocity is rendered for the increasing squeezing factor i.e. the separation of the plates gives rise to an increase in the fluid velocity but the rate of enhancement in the case of water is less than that of kerosene.
- Fluid velocity shows a dual characteristic for the enhanced velocity slip and the result reveals that for the increasing slip the fluid velocity retards near the low plate and is reversed at the upper.
- The existence of the Hartmann number favors enhancing the velocity at the lower plate and the impact is opposite at the upper plate.
- The additional heat source provided by the space and temperature-dependent both favors in hike of the fluid temperature within the entire domain.
- The coupling effect due to the dissipative heat i.e. the increasing Eckert number enhances the heat transport properties but it has greater control over the heat transfer rate,
- The impact of thermal radiation for the occurrence of the radiative heat flux significantly enhances the heat transfer rate for both the case of water/kerosene nanofluid.

However, future investigation can enhance the study by incorporating a comparative analysis for the incorporation of various nanoparticles in place of Copper with base fluid like ethylene glycol, bio-based oil, etc. Further, focus on optimizing the concentration of nanoparticles in nanofluids for various conditions. The use of Riga plates introduces electromagnetic fields to control fluid flow is one of the important approaches for the future study. New analytical method can be implemented to get the solution of the model and a comparative analysis would be a great approach. Although the present investigation provides numerical treatment using the spectral quasilinearization method, experimental validation of the proposed results would be crucial. Future work could involve designing experimental setups to benchmark the performance of nanofluids in similar conditions, helping to verify the theoretical predictions and extend the findings to real-world systems (Table 5).

Funding

Not applicable.

Availability of data and material

No data is used.

Authors' contributions

All the authors have equally contributed to complete the manuscript, i.e. SP has formulated the problem and TMA verified the problem statement, RB has completed the draft with results and discussion section and SRM checked the overall.

Ethics approval

The entire work is the original work of the authors.

Consent to participate

Not applicable.

Consent for publication

All the authors have given their consent to publish the paper.

Declaration of competing interest

The authors declare that they have no known competing financial interests or personal relationships that could have appeared to influence the work reported in this paper.

Data availability

No data was used for the research described in the article.

References

1. Choi SU, Eastman JA. *Enhancing Thermal Conductivity of Fluids with Nanoparticles (No. ANL/MSD/CP-84938; CONF-951135-29)*. Argonne, IL (United States): Argonne National Lab.(ANL); 1995.
2. Mahboobtosi M, Hosseinzadeh K, Ganji DD. Investigating the convective flow of ternary hybrid nanofluids and single nanofluids around a stretched cylinder: parameter analysis and performance enhancement. *Int J Thermofluids*. 2024;23, 100752.
3. Yasir M, Malik ZU, Alzahrani AK, Khan M. Study of hybrid Al2O3-Cu nanomaterials on radiative flow over a stretching/shrinking cylinder: comparative analysis. *Ain Shams Eng. J*. 2023;14(9), 102070.
4. Khan WA, EL-Hakiem AMA, Nabwey HA, Rashad AM, Sayed G. Heat and mass transfer of Williamson and Maxwell micropolar nanofluid over a wedge with magnetic field and activation energy effects. *Partial Differ Equ Appl Math*. 2024;11, 100796.
5. Krishna MV, Chamkha AJ. Hall and ion slip effects on MHD rotating boundary layer flow of nanofluid past an infinite vertical plate embedded in a porous medium. *Results Phys*. 2019;15, 102652.
6. Hayat T, Khan M, Imtiaz M, Alsaedi A. Squeezing flow past a Riga plate with chemical reaction and convective conditions. *J Mol Liq*. 2017;225:569–576.
7. Ahmed N, Khan U, Mohyud-Din ST. Influence of thermal radiation and viscous dissipation on squeezed flow of water between Riga plates saturated with carbon nanotubes. *Colloids Surf A Physicochem Eng Asp*. 2017;522:389–398.
8. Kumar M, Kaswan P, Kumari M, Ahmad H, Askar S. Cattano Christov double diffusion model for third grade nanofluid flow over a stretching Riga plate with entropy generation analysis. *Heliyon*. 2024;10(10).
9. Khan SA, Waqas H, Naqvi SMRS, Alghamdi M, Al-Mdallal Q. Cattaneo-Christov double diffusions theories with bio-convection in nanofluid flow to enhance the efficiency of nanoparticles diffusion. *Case Stud Therm Eng*. 2021;26, 101017.
10. Sarfraz M, Khan M. Rheology of gyrotactic microorganisms in Jeffrey fluid flow: a stability analysis. *Mod Phys Lett B*. 2024;38(05), 2450003.
11. Hayat T, Ullah I, Muhammad K, Alsaedi A. Gyrotactic microorganism and bio-convection during flow of Prandtl-Eyring nanomaterial. *Nonlinear Eng*. 2021;10(1): 201–212.
12. Salahuddin T, Kalsoom SM, Awais M, Khan M, Altanji M. Impact of Darcy-Forchheimer for the flow analysis of radiated tangent hyperbolic fluid with viscous dissipation and activation energy. *Int J Hydrogen Energy*. 2024;72:949–957.
13. Awais M, Salahuddin T, Muhammad S. Effects of viscous dissipation and activation energy for the MHD Eyring-powell fluid flow with Darcy-Forchheimer and variable fluid properties. *Ain Shams Eng J*. 2024;15(2), 102422.
14. Rasool G, Zhang T. Darcy-Forchheimer nanofluidic flow manifested with Cattaneo-Christov theory of heat and mass flux over non-linearly stretching surface. *PLoS One*. 2019;14(8), e0221302.
15. Dero S, Shaikh H, Talpur GH, Khan I, Alharbim SO, Andualem M. Influence of a Darcy-Forchheimer porous medium on the flow of a radiative magnetized rotating hybrid nanofluid over a shrinking surface. *Sci Rep*. 2021;11(1):24257.
16. Eswaramoorthi S, Thamaraiselvi S, Loganathan K. Exploration of Darcy–Forchheimer flows of Non-Newtonian Casson and Williamson conveying tiny particles experiencing binary chemical reaction and thermal radiation: comparative Analysis. *Math Comput Appl*. 2022;27(3):52.
17. Mishra SR, Agbaje TM, Baithalu R, Panda S. Spectral quasi-linearization approach for the swimming of motile microorganisms on the bio-convection Casson nanofluid flow over a rotating circular disk. *Numerical Heat Transfer, Part B: Fundamentals*. 2024:1–27.
18. Agbaje TM, Baithalu R, Mishra SR, Panda S. Irreversibility Processes on the Squeezing Flow Analysis of Blood-Based Micropolar Hybrid Nanofluid Through Parallel Channel: spectral Quasilinearisation Method. *Bionanoscience*. 2024:1–15.
19. Panda S, Pattnaik PK, Baithalu R, Mishra SR. Inertial drag combined with non-uniform heat generation/absorption effects on the hydromagnetic flow of polar nanofluid over an elongating permeable surface due to the impose of chemical reaction. *ZAMM-Journal of Applied Mathematics and Mechanics/Zeitschrift für Angewandte Mathematik und Mechanik*. 2024, e202301058.
20. Mishra SR, Panda S, Baithalu R. Enhanced heat transfer rate on the flow of hybrid nanofluid through a rotating vertical cone: a statistical analysis. *Partial Differ Equations Appl Math*. 2024;11, 100825.
21. Bellman RE, Kalaba RE. *Quasilinearization and Nonlinear Boundary-Value Problems. Modern Analytic and Computational Methods in Science and Mathematics*. Elsevier; 1965.
22. Motsa SS. A new spectral local linearization method for nonlinear boundary layer flow problems. *J Appl Math*. 2013. https://doi.org/10.1155/2013/423628. Article ID 423628.
23. Hayat T, Khan M, Imtiaz M, Alsaedi A. Squeezing flow past a Riga plate with chemical reaction and convective conditions. *J Mol Liq*. 2017;225:569–576.
24. Zeeshan A, Arain MB, Bhatti MM, Alzahrani F, Bég OA. Radiative bioconvection nanofluid squeezing flow between rotating circular plates: semi-numerical study with the DTM-Padé approach. *Mod Phys Lett B*. 2022;36(03), 2150552.
25. Yusuf A, Akolade MT, Tijani YO. Nonlinear Mixed Convective Analysis of Thomson and Troian Slip Flow Conditions for Ag–Cu–TiO2/H2O Hybrid Nanofluid Over a Riga Plate. *J Comput Theor Transp*. 2024:1–22.
26. Yusuf, A., Adekunle, T.S., Tiamiyu, A.T., & Aliyu, A.M. (2023). Double Diffusive Nonlinear Convective MHD Unsteady Slip-Flow Regime in a Rectangular Channel.
27. Ali B, Jubair S, Fouly A. Heat and mass transmission through the nanofluids flow subject to exponential heat source/sink and thermal convective condition across Riga plates. *Chem Eng Res Des*. 2024;207:458–465.
28. Batchelor GK. The effect of Brownian motion on the bulk stress in a suspension of spherical particles. *J Fluid Mech*. 1977;83(1):97–117.
29. Mintsa HA, Roy G, Nguyen CT, Doucet D. New temperature dependent thermal conductivity data for water-based nanofluids. *Int J Therm Sci*. 2009;48(2):363–371.